Physics and Imaging in Radiation Oncology 11 (2019) 1–8

Contents lists available at ScienceDirect

Physics and Imaging in Radiation Oncology

journal homepage: www.elsevier.com/locate/phro

Original Research Article

Assessment of dosimetric and positioning accuracy of a magnetic resonance imaging-only solution for external beam radiotherapy of pelvic anatomy

Reko Kemppainen[a,b,*], Sami Suilamo[c,d], Iiro Ranta[c,d], Marko Pesola[a], Aleksi Halkola[a], Alvin Eufemio[a], Heikki Minn[d], Jani Keyriläinen[c,d]

[a] Philips Oy, Äyritie 4, FI-01510 Vantaa, Finland
[b] Department of Neuroscience and Biomedical Engineering, Aalto University School of Science, Rakentajanaukio 2 C, FI-02150 Espoo, Finland
[c] Department of Medical Physics, Turku University Hospital, Hämeentie 11, P.O. Box 52, FI-20521 Turku, Finland
[d] Department of Oncology and Radiotherapy, Turku University Hospital, Hämeentie 11, P.O. Box 52, FI-20521 Turku, Finland

ARTICLE INFO

Keywords:
Radiotherapy
MRI-only
Image-guided radiotherapy
Position verification

ABSTRACT

Background and purpose: The clinical feasibility of synthetic computed tomography (sCT) images derived from magnetic resonance imaging (MRI) images for external beam radiation therapy (EBRT) planning have been studied and adopted into clinical use recently. This paper evaluates the dosimetric and positioning performance of a sCT approach for different pelvic cancers.

Materials and methods: Seventy-five patients receiving EBRT at Turku University Hospital (Turku, Finland) were enrolled in the study. The sCT images were generated as part of a clinical MRI-simulation procedure. Dose calculation accuracy was assessed by comparing the sCT-based calculation with a CT-based calculation. In addition, we evaluated the patient position verification accuracy for both digitally reconstructed radiograph (DRR) and cone beam computed tomography (CBCT) -based image guidance using a subset of the cohort. Furthermore, the relevance of using continuous Hounsfield unit values was assessed.

Results: The mean (standard deviation) relative dose difference in the planning target volume mean dose computed over various cancer groups was less than 0.2 (0.4)% between sCT and CT. Among all groups, the average minimum gamma-index pass-rates were better than 95% with a 2%/2mm gamma-criteria. The difference between sCT- and CT-DRR-based patient positioning was less than 0.3 (1.4) mm in all directions. The registrations of sCT to CBCT produced similar results as compared with CT to CBCT registrations.

Conclusions: The use of sCT for clinical EBRT dose calculation and patient positioning in the investigated types of pelvic cancers was dosimetrically and geometrically accurate for clinical use.

1. Introduction

Computed tomography (CT) is currently the primary imaging modality for providing anatomical and tissue density information in the external beam radiation therapy (EBRT) planning of pelvic cancers. Magnetic resonance imaging (MRI) is widely used as a supplement to the CT imaging [1–3]. The most significant advantage of MRI over CT is its better soft-tissue contrast, which results in a more accurate gross tumor volume and organ at risk (OAR) delineation [4–7]. Additional benefits include the usage of non-ionizing radiation and the versatility of acquisition sequences allowing the cancer- or organ-specific imaging methods [5].

A major drawback of multi-modality imaging in EBRT is the residual registration error remaining when the images from two or more modalities are registered with each other [8]. Recent advances in the use of MRI promise to eliminate the registration error by using only the MR images for planning and dose calculation in the EBRT of prostate and brain cancer (see the recent reviews [9–11]). In an MRI-only workflow, so-called synthetic CT (sCT) images are generated from the magnetic resonance (MR) images, providing the tissue density information for dose calculation and reference images for patient position verification. Over recent years, commercial solutions for obtaining the sCT for prostate cancer patients have been introduced [12,13].

A commercially available solution for the sCT generation was used in this work. It has been shown that the solution can be used for an accurate dose calculation and patient positioning for prostate cancer patients [13,14]. In addition, its feasibility for other indications in the pelvic anatomy was demonstrated in our earlier study [15]. However,

* Corresponding author at: Philips Oy, Äyritie 4, FI-01510 Vantaa, Finland.
E-mail address: reko.kemppainen@gmail.com (R. Kemppainen).

https://doi.org/10.1016/j.phro.2019.06.001
Received 26 October 2018; Received in revised form 30 May 2019; Accepted 2 June 2019

the bulk assignment of Hounsfield unit (HU) values limits the soft-tissue characterization, and consequently affects the ability to verify treatment position based on a tissue contrast. In addition, the sCT methods suitable for prostate EBRT may not be directly applicable to other pelvic targets due to larger treatment volumes and higher patient demographic variability, both characteristic for the non-prostate pelvic cancer. Thus, additional validation of a sCT solution for general pelvic imaging is required.

The feasibility of sCT methods for general pelvic anatomy including the assessment of both dosimetric and positioning accuracy have not been studied within a single study. Several groups have assessed the dosimetric and positioning for prostate cancer with comparison of continuous HU and bulk HU assignment (see e.g. [16–19]). Two recent studies have evaluated the feasibility of MRI-only workflow for rectal cancers [20,21]. However, to the best of our knowledge, only the dosimetric accuracy has been evaluated for gynecological cancers [22–24].

The aim of this study was to evaluate the feasibility of an MRI-only method in terms of dose calculation, position verification and geometric accuracy in EBRT for the pelvic anatomy in general. In addition, we have evaluated the necessity of continuous HU values in sCT images for dosimetric and positioning accuracy for prostate cancer patients. This research addressed the use of sCT in pelvis which included the cone beam computed tomography (CBCT)- and digitally reconstructed radiograph (DRR)-based position verification workflows. Furthermore, both bone- and soft-tissue-based registration workflows for CBCT were evaluated.

2. Materials and methods

2.1. Patient cohort and image acquisition

The study cohort consisted of 75 consecutive patients referred to EBRT of pelvic cancers at the Department of Oncology and Radiotherapy of Turku University Hospital in Turku, Finland. The patients were enrolled in between October 2017 and August 2018. The Ethical Committee of the Hospital District of Southwest Finland approved the study, and an informed consent was obtained (reference code: Dnro 116/1801/2017).

There were 20 (27%) female and 55 (73%) male patients divided into five groups each consisting of 15 patients. A total of 45 (60%) patients had a prostate cancer of whom 15 underwent definitive, 15 postoperative, and 15 regional pelvic lymph node EBRT. The remaining two groups consisted of 15 patients with rectal and 15 patients with gynecological cancer, respectively (see the Table 1 for further details).

The CT simulation images were acquired using the Aquilion LB (Toshiba Corp., Tokyo, Japan) scanner with 2-mm-thick slices, $1 \times 1\,mm^2$ in-plane resolution, 120 kV tube voltage, and tube current modulation in cranio-caudal (CC) direction (Toshiba Sure-Exposure 3D SD 12.50). The MR images were recorded with the Ingenia 1.5T HP (sw. version 5.3.1, Philips MR Medical Systems International B.V., Best, Eindhoven, The Netherlands) scanner. For all patients, an axial T1-weighted three-dimensional (3D) mDIXON sequence [13] was acquired covering the full body contour (see the Supplementary Table 1 for MRI parameters). The MR images were used as a source for the sCT generation. Patients were positioned similarly during the imaging for CT and MRI simulation using the same patient positioning devices (including knee support) as during treatment. During the MRI scan, patients were placed in a supine position on a flat EBRT couch top and an anterior MRI-coil was placed above the imaging volume using a coil holder to prevent body outline deformation.

The planar radiograph and CBCT positioning images were acquired with the on-board imager system integrated to a linear accelerator (Varian Medical Systems Inc., Palo Alto, CA, USA). In the DRR study, two orthogonal projections (anterior-posterior (AP) or posterior-anterior (PA); and left–right (LR) or right-left (RL)) were obtained for all patients with a pixel size of $0.388 \times 0.388\,mm^2$; a field-of-view (FOV) of $30 \times 40\,cm^2$. For volumetric imaging, the CBCT images were acquired using 125 kV and 80 mAs with a $1 \times 1\,mm^2$ in-plane resolution, 2-mm-thick slices and 160 mm coverage.

2.2. Synthetic CT generation

Two different versions of the sCT generation method (Magnetic Resonance for Calculating Attenuation, MRCAT, Philips Oy, Vantaa, Finland) were used in this study. The first version used a bulk assignment of HU values, which is referred to as sCTb in this study. The second version was an improved version of the MRCAT providing continuous HU values called sCTc hereafter. In the subgroup of patients receiving the radical treatment for prostate cancer (N = 15), both versions were generated for comparison of the methods. For other four cancer groups, only the sCTc was generated to evaluate the new method.

In the sCTb generating algorithm, the CT-like density maps were computed from the mDIXON MR images in a two-step approach [13,25,26]. In the first step, the content of the MR image was categorized into five classes. In the second step, each voxel was assigned the following HU: spongy bone (198 HU), compact bone (949 HU), fat (-86 HU), and water-rich tissue (42 HU).

The sCTc and sCTb used the segmentation of bones and soft-tissue based on mDIXON MR images. However, instead of the bulk assignment, the continuous HU values were used based on fat/water fraction within the voxels. In addition, the voxels on the body outline could partially contain air for modeling the partial volume effect. The sCTc images were obtained from the manufacturer while the sCTb images were generated at the scanner console. See the electronic supplementary material for details of the sCT generation.

2.3. Image processing

The CT images were rigidly registered to the sCTc and resampled to the same pixel grid using B-spline interpolation with the Elastix 4.9.0 [27] program. The registration parameters were the same used by Maspero et al. [28] for the registration between CT and sCT images. In CT images, the air cavities in the bowel and rectum were filled for all patients with 0 HU using the Matlab scripts (MATLAB® 8.4.0.150421 (R2014b), The MathWorks Inc., Natick, MA, USA). The filling was equivalent to density override by water in the treatment planning

Table 1
Patient demographics and structure details within five different cancer groups (mean (standard deviation)) (PTV: planning target volume).

	Pelvic lymph node	Rectal cancer	Gynecological cancer	Prostate post-operative	Prostate definitive
Patient demographics					
Average age (years)	65.7 (6.2)	68.2 (10.6)	67.3 (14.0)	68.7 (6.8)	70.3 (8.0)
Sex (males/females)	15/0	10/5	0/15	15/0	15/0
Structure details					
PTV volume (cm^3)	1233 (4 4 3)	1621 (6 1 1)	1340 (7 1 6)	376 (1 0 2)	130 (43)
Bladder volume (cm^3)	231 (1 3 9)	287 (1 8 9)	225 (1 1 8)	239 (1 2 4)	281 (2 2 9)
Rectum volume (cm^3)	92 (41)	155 (34)	86 (43)	78.84 (37)	91 (43)

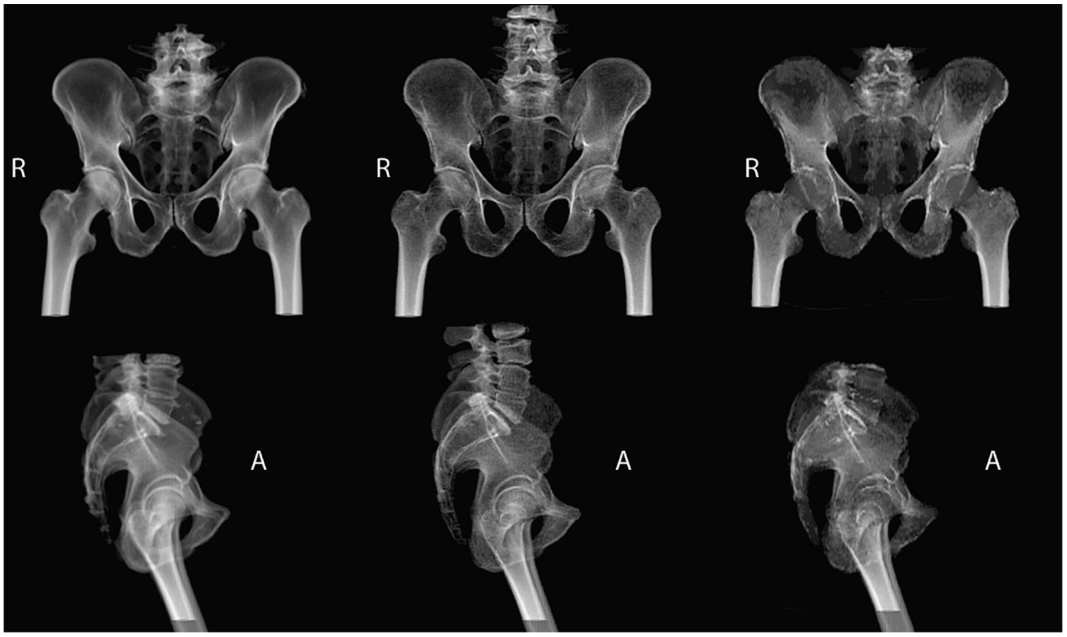

Fig. 1. Example DRR images from Eclipse treatment planning system using bone rendering (HU values less than 100 and above 1000 omitted). CT (left), sCTc with continuous HU values (middle), and sCTb with discrete HU values, (right) (DRR: digitally reconstructed radiograph, HU: Hounsfield unit, CT: computed tomography, sCT: synthetic computed tomography, R: right, A: anterior).

system (TPS) corresponding to a clinical practice used with patients encompassing large air volumes at our institution. The same approach was used [20] or suggested to be used [29] in the dosimetric evaluations of MRI-only methods in order to avoid confounding dosimetric differences not related to the sCT methods.

2.4. Dose calculation accuracy

The dosimetric agreement between planning CT and sCT was evaluated by recalculating the clinical plans in the Eclipse 13.6 (Varian Medical Systems Finland Oy, Helsinki, Finland) TPS using the sCT for inhomogeneity correction, an anisotropic analytical algorithm (AAA) for dose computation and a volumetric modulated arc (VMAT) delivery technique. The voxel grid size for optimization and dose calculation was set to $2.0 \times 2.0 \times 2.0\,mm^3$. The dosimetric agreement between CT and sCT was evaluated per cancer group for all patients. The evaluation metrics included dose-volume histogram (DVH) comparison for the PTV and OARs, 3D gamma analysis and dose comparison statistics.

The DVH evaluation was based on the structures that were copied from the planning CT to sCT based on rigid registration. Minimum, median and maximum ($D_{2\%}$, $D_{50\%}$, $D_{98\%}$) dose points were evaluated for the PTVs while volumes of $V_{95\%}$ and $V_{70\%}$ were assessed for the OARs. The results were computed as a relative difference with respect to prescribed dose $\left(\frac{D(pCT)-D(CT)}{D_{presc.}}\right)$ for dose points or structure volume $\left(\frac{V(pCT)-V(CT)}{V_{struct.}}\right)$ for volume points.

The 3D gamma analysis was performed using the Plastimatch 1.7.3 (http://plastimatch.org/index.html) open source software for image registration. Various gamma-index pass-rate criteria and dose cut-off values were evaluated using a global gamma-index relative to the maximum dose. The maximum value of gamma-index to compute was set to the default value of two.

2.5. Image similarity and body outline distortion

The differences between CT and sCT images were evaluated by computing a mean absolute error (MAE) and a mean error (ME) between the HU values within the intersection of the body contours of the two images. In addition, to assess the body outline correctness in sCT, the difference between CT and sCT body outline was computed for different CC positions at the distances from −150 to 150 mm from the MRI scanner isocentre. Furthermore, the computed body outline differences were compared with the measured geometric distortion to assess the origin of the differences in body outline.

The assessment of image similarity and body outline was performed using a Matlab program. First, the program evaluated the body outline difference at each CC-position for all patients as function of angle. Then the information at each CC-location was condensed by computing the mean absolute difference and standard deviation of the mean absolute difference over all angles and patients.

The MRI-system induced geometric distortions were evaluated by imaging a large 3D phantom containing a regular grid of MRI-positive markers. The parameters of the imaging sequence affecting geometric accuracy (sequence type and receiver bandwidth) were matched with the sCT source image. First, the markers were located, and their positions were compared with the phantom structure in order to compute the geometric distortion at the marker locations. Then, for each included patient, the obtained distortion map was interpolated to the positions defining the body outline structure. Finally, the geometric distortion was evaluated over a study cohort (see a detailed description in [15]).

2.6. Positioning accuracy and precision

A subset of the cohort was selected for the assessment of both the DRR- and CBCT-based position verification before each treatment fraction.

2.6.1. DRR

In the DRR study, 20 consecutive patients were selected consisting of nine females with three rectum and six gynecological cancer patients and eleven males with seven prostate and four rectum cancer patients. The manual registrations between CT-DRR and planar radiograph were compared with the manual registrations between sCT-DRR to planar radiograph (see the Fig. 1 for visualization of DRRs and Supplementary Fig. 1 for visualization of performed registrations). The manual

Table 2
Dose-volume histogram (DVH) comparison for all five pelvic cancer groups and comparison between two synthetic computed tomography (sCT) versions ($\frac{\mathbf{sCT-CT}}{\mathbf{CT_{ref}}}$, mean relative difference (SD, standard deviation) [range]) including the planning target volume (PTV), rectum and bladder, gamma analysis, dose statistics ($\frac{\mathbf{sCT-CT}}{\mathbf{CT}}$, mean relative difference (SD)), gamma-index pass-rates (mean (SD) [range]), and Hounsfield unit (HU) similarity evaluation (mean (SD) [range]). $V_{X\%}$ indicates the volume, where the dose is higher than X% of the prescribed dose. For DVH comparison, the CT_{ref} is either prescribed dose (for $D_{X\%}$) or structure volume (for $V_{X\%}$). For dose statistics per volume and PTV mean dose, values are relative to respective value obtained using CT. MAE: mean absolute error, ME: mean error.

	Pelvic lymph nodes (n = 15)	Rectal cancer (n = 15)	Gynecological cancer (n = 15)	Prostate cancer, post-operative (n = 15)	Prostate cancer, definitive (continuous HU, n = 15)	Prostate cancer, definitive (bulk HU, n = 15)
DVH comparison						
PTV						
Mean	0.0 (0.4) [−0.5 − 0.8]	0.1 (0.3) [−0.4 − 0.6]	−0.2 (0.4) [−1.0 − 0.3]	0.1 (0.3) [−0.4 − 0.6]	0.1 (0.2) [−0.2 − 0.4]	0.1 (0.2) [−0.5 − 0.3]
$D_{2\%}$	0.1 (0.5) [−0.6 − 1.2]	0.5 (0.6) [−0.7 − 2.0]	0.1 (0.4) [−0.7 − 0.7]	0.2 (0.6) [−0.4 − 2.0]	0.1 (0.2) [−0.3 − 0.4]	0.1 (0.2) [−0.6 − 0.4]
$D_{50\%}$	0.0 (0.4) [−0.6 − 0.8]	0.1 (0.3) [−0.3 − 0.5]	−0.2 (0.4) [−1.1 − 0.3]	0.0 (0.3) [−0.4 − 0.4]	0.1 (0.2) [−0.3 − 0.4]	0.1 (0.2) [−0.6 − 0.4]
$D_{98\%}$	−0.1 (0.3) [−0.9 − 0.5]	0.0 (0.4) [−1.0 − 0.4]	−0.2 (0.5) [−1.1 − 0.8]	0.0 (0.3) [−0.5 − 0.5]	0.1 (0.3) [−0.3 − 0.5]	0.1 (0.2) [−0.5 − 0.4]
Rectum						
$V_{95\%}$	0.1 (0.3) [−0.3 − 0.5]		−0.2 (1.8) [−4.9 − 3.2]	0.1 (0.4) [−0.4 − 0.8]	0.1 (0.1) [−0.1 − 0.2]	0.1 (0.1) [−0.1 − 0.3]
$V_{75\%}$	0.0 (0.1) [−0.3 − 0.2]		−0.3 (0.6) [−1.7 − 0.5]	0.0 (0.2) [−0.2 − 0.4]	0.0 (0.1) [−0.1 − 0.1]	0.0 (0.1) [−0.1 − 0.1]
Bladder						
$V_{95\%}$	−0.1 (0.3) [−0.6 − 0.7]	0.1 (0.5) [−0.6 − 1.2]	−0.1 (0.9) [−2.8 − 0.9]	−0.1 (0.2) [−0.3 − 0.3]	0.0 (0.2) [−0.7 − 0.3]	0.0 (0.2) [−0.7 − 0.2]
$V_{75\%}$	0.0 (0.2) [−0.2 − 0.5]	0.1 (0.2) [−0.2 − 0.6]	0.0 (0.2) [−0.2 − 0.3]	0.0 (0.1) [−0.1 − 0.1]	0.0 (0.1) [−0.3 − 0.2]	0.0 (0.1) [−0.4 − 0.1]
Gamma statistics (V10)						
2%2mm	97.7 (0.7) [96.0 − 99.3]	96.2 (2.0) [91.3 − 97.8]	97.0 (1.5) [93.0 − 98.7]	98.0 (0.6) [96.7 − 98.8]	99.1 (0.5) [97.7 − 99.7]	98.9 (0.4) [97.8 − 99.6]
Dose statistics per volume						
$V_{10\%}$	0.0 (0.2) [−0.5 − 0.2]	0.1 (0.3) [−0.5 − 0.5]	−0.1 (0.3) [−0.9 − 0.3]	−0.1 (0.2) [−0.4 − 0.2]	−0.1 (0.2) [−0.4 − 0.2]	−0.3 (0.2) [−0.6 − −0.1]
HU-similarity						
MAE	49.1 (4.0) [42.8 − 54.3]	48.6 (2.8) [44.3 − 54.3]	47.7 (7.3) [37.1 − 67.5]	48.9 (3.6) [43.8 − 57.4]	47.4 (3.8) [42.6 − 54.2]	48.0 (5.7) [41.5 − 59.8]
ME	−4.6 (4.1) [−9.7 − 3.6]	−5.3 (4.6) [−14.1 − 2.2]	−6.6 (3.1) [−13.4 − −1.4]	−4.5 (3.4) [−9.9 − 1.1]	−5.7 (4.2) [−14.7 − 3.5]	7.2 (4.1) [−0.9 − 16.1]

registrations were performed using a Matlab-based tool simulating the paired registration of planar kV and DRR images. The observers were asked to perform manual registrations of the paired projections shown to them in random order. The clinical set-up correction protocols per cancer type were not used but all of the cases were registered using the same procedure.

In total, five observers (two medical physicists and three radiographers) performed registrations with three replications of each registration (20 cases × 2 methods × 3 repetitions = 120 number of registrations per observer). In addition, for seven prostate cancer patients both sCTc and sCTb were evaluated to compare the relevance of continuous HU versus bulk HU assignment in the sCT generation (adding 7 cases × 1 method × 3 repetitions = 21 registrations per observer). The fraction used was randomly chosen.

The assessment of positioning accuracy was performed by computing the mean and standard deviation (SD) of the difference of registrations obtained by CT-DRR and sCT-DRR.

2.6.2. CBCT

The CBCT-based verification of patient position was studied by comparing the registrations between CT to CBCT and sCT to CBCT relying on either bony structures or soft-tissue contrast for a subset of ten patients. In each registration methods, ten consecutive patients with a randomly chosen fraction were selected and the registration between the images were performed in the Offline Review module of Eclipse TPS. The registration was restricted to translations corresponding to the treatment couch movements available in the linac.

The performance of the bone-based registration was assessed as a difference between CT and sCT positioning. The observer was instructed to position the patient using automatic registration tools like prior to the treatment. Both PTV and OAR structures were visible during the registration. The bone registration study cohort consisted of four women with gynecological cancer and six men receiving treatment for post-operative prostate cancer.

In the evaluation of soft-tissue-based position verification, two datasets were prepared using the data from the radical prostate cancer group. The first set contained original CT, sCT and CBCT images, where the fiducial markers were visible in the images directly or as contours. In the second set, the markers were removed from CT, sCT and CBCT images using the Photoshop 6 (Adobe Inc., City of San José, CA, USA) image processing tool. First, the DICOM (digital imaging and communications in medicine) images were imported as 16-bit images enabling preservation of the data using the functionality integrated to the Photoshop. Then, the seeds were manually removed using the patch and healing brush tools. After removal, the images were stored as 16-bit TIFF (tagged image file format) images and again as DICOM images using Matlab. Finally, the images were imported back to the TPS for registration. Three evaluators performed registrations for both image sets (see the Supplementary Fig. 2) and the difference between marker-based and soft-tissue-based registration was used as a goodness metric of registration for both modalities independently.

2.7. Statistical analysis

Statistical analysis was conducted using Minitab (version 17, Minitab Inc., State College, PA, USA) numerical analysis software. The data between sCTc and sCTc were tested whether the means of the two dependent groups differ using the two-sample *t*-test.

3. Results

3.1. Dose difference

The mean (SD) dose differences of the PTV mean dose computed over cancer groups, each with 15 patients, were less than 0.2 (0.4)% between sCTc and CT. The mean dose differences for studied volumes were less than −0.3 (0.6)% (see the Table 2) for OARs. Two outliers for the rectum DVH comparison were identified in the gynecological cancer group. Without including the two outliers, the difference for the rectum V95% was −0.1 (0.8)% [−1.1–1.3] (for visualization of the outlier DVHs see the electronic supplementary material).

The mean gamma-index pass-rate evaluation was highest for the prostate cancer patients and lowest for the gynecological and rectal cancer patients. Among all groups, the average pass-rates within volumes of $V_{10\%}$ were higher than 95% with 2%/2mm gamma-criteria. The lowest pass-rate was for the rectum cancer group being 96.2 (2.0)%. The mean relative dose differences were less than 0.3 (0.3)% for all studied cancer groups and volumes of interest. The MAE was less than 50 HU for all studied cancer groups (see the Table 2).

An example of gynecological cancer patient is illustrated in the Supplementary Fig. 4. More comprehensive set of results are presented in the online supplementary material (see the Supplementary Table 2).

3.2. Bulk to continuous HU comparison

For prostate cancer patients, the mean (SD) dose difference, within a volume receiving more than 10% of the prescribed dose, was −0.1 (0.2)% and −0.3 (0.2)% for sCTb and sCTc, respectively. Statistically significant differences were observed in the mean error (ME, $p < 0.01$) of HU values, mean dose within $V_{10\%}$ ($p < 0.01$) and mean gamma-index pass-rates with 2%/2mm gamma-criteria ($p = 0.04$) (see the Supplementary Table 4).

3.3. Body outline and geometric analysis

The body outline differences and the MRI-system-induced geometric distortion were the smallest close to the isocentre of MRI device. Nearby the isocentre, the absolute difference of body outline between CT and sCTc was 2 mm on average, but it increased farther away from the isocentre and reached the average difference of 6 mm at 150 mm (see the Fig. 2). The contribution of geometric distortion to the body outline difference was less than 2 mm within the investigated volumes.

The systematic difference between CT and sCTc body outlines was observed for various CC distances from the isocentre of MRI device (see

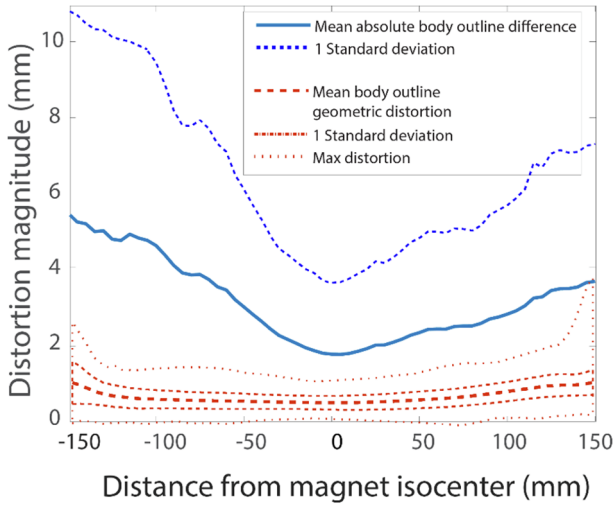

Fig. 2. Mean absolute body outline difference (solid blue line) and mean + 1SD (dash-dotted line) between CT and sCT images. Mean body outline geometric distortion (dashed red line), mean + 1SD (red dashed-dotted) and max distortion (red dashed line) of the body outline due to geometric distortions of MR images as a function of (cranio-caudal) distance from the isocentre of MRI device (SD: standard deviation, CT: computed tomography, sCT: synthetic computed tomography, MRI: magnetic resonance imaging). (For interpretation of the references to colour in this figure legend, the reader is referred to the web version of this article.)

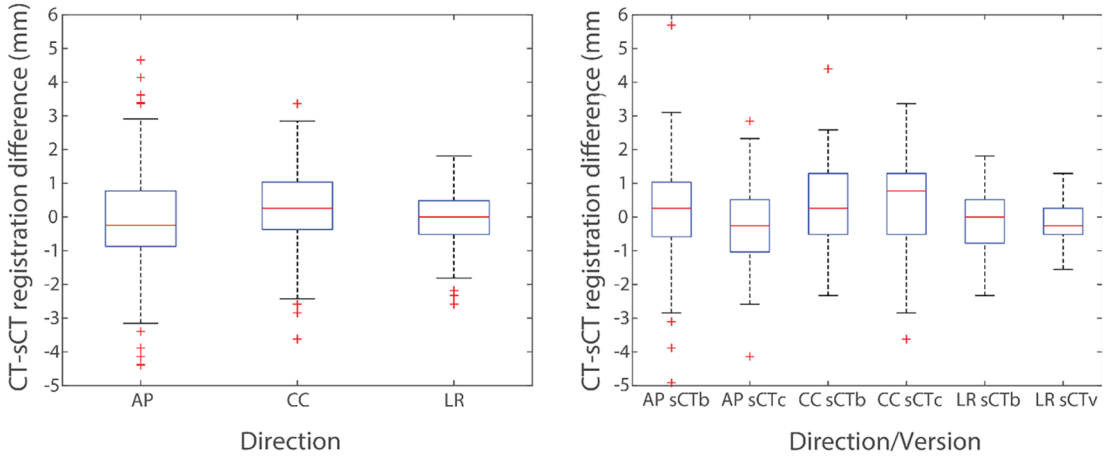

Fig. 3. *Left:* Box-plot of differences between CT-DRR to planar kV-image and sCTc-DRR to planar kV-image registration for anterior-posterior (AP), cranio-caudal (CC) and left–right (LR) directions evaluated using a group of 20 patients. *Right*: Box-plot of difference between CT-DRR to planar kV-image and sCT-DRR to planar kV-image registration for AP, CC and LR directions evaluated for bulk HU (sCTb) and continuous HU (sCTc) sCT evaluated using a subset of seven patients. (CT: computed tomography, DRR: digitally reconstructed radiograph, kV: kilovoltage, sCT: synthetic computed tomography, HU: Hounsfield unit).

the Supplementary Fig. 3). The largest systematic differences were present toward the cranial end of the studied FOV at angles corresponding patient's anterior direction (angle 0°). Towards the caudal end, systematic differences were not found, but the random uncertainty increased.

3.4. Positioning

3.4.1. DDR positioning

The mean (SD) difference between CT- and sCTc-based DRR positioning evaluated for 20 patients was −0.1 (1.4) mm, 0.3 (1.1) mm and 0.1 (0.8) mm, in AP, CC and LR direction, respectively (see Fig. 3).

The comparison of sCTb and sCTc was performed using subset of 7 patients. The mean (SD) difference between CT- and sCTc-based DRR positioning was −0.2 (1.2) mm, 0.4 (1.3) mm and −0.1 (0.6) mm, in AP, CC and LR direction, respectively. For sCTb, the difference was 0.2 (1.6) mm, 0.3 (1.2) mm and −0.1 (0.9) mm, respectively.

3.4.2. CBCT positioning

For the bone-based positioning studied with ten patients, the mean (SD) observer differences were 0.1 (1.1) mm, 0.1 (0.6) mm and −0.0 (0.2) mm in AP, CC and LR directions, respectively (see the Fig. 4).

For the soft-tissue-based positioning in the AP direction, the mean (SD) differences between fiducial markers- and soft-tissue-based registrations were 0.5 (1.8) mm, 0.5 (1.8) mm and 1.1 (1.8) mm for CT, sCTc and sCTb, respectively. In the CC direction, the mean (SD) differences were −0.2 (1.1) mm, −0.6 (1.3) mm and −0.8 (2.3) mm, respectively. Furthermore, the smallest registration differences were seen in the LR direction, being 0.1 (0.7) mm, −0.4 (0.7) mm and −0.2 (0.6) mm for CT, sCTc and sCTb, respectively.

4. Discussion

Pelvic cancer patients would benefit from the use of sCT in terms of decreased total uncertainties in EBRT [22–24]. This study aimed at demonstrating dosimetric and positioning accuracy of using MRCAT sCT with continuous HU values for the EBRT of pelvic cancers. This study covered several possible positioning workflows that have not been assessed previously. The results were relevant when aiming to extend the use of sCT method to pelvic cancer patients.

The dosimetric accuracy was assessed by comparing sCT to CT-based dose computation. The dosimetric differences between CT and sCTc were found to be small among all cancer groups. Considering mean (SD) gamma-index pass-rates of 98.0 (0.6)%, 96.2 (2.0)% and

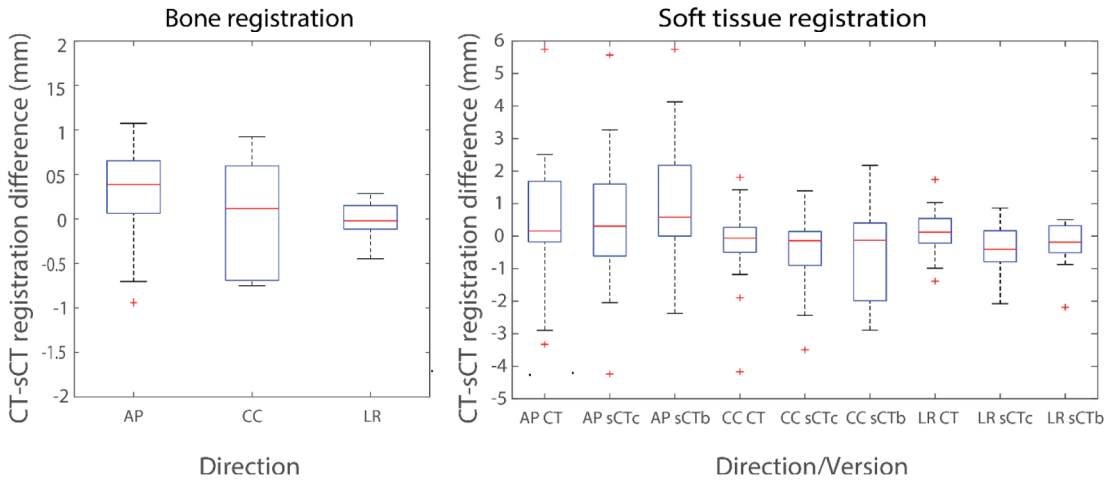

Fig. 4. *Left:* Box-plot of registration difference between CT-to-CBCT and sCTb-to-CBCT using bone-based registration in left–right (LR), anterior-posterior (AP) and cranio-caudal (CC) direction. *Right:* Box-plot of registration differences between CT to CBCT and sCT to CBCT using soft-tissue contrast with respect to marker-based registration in AP, CC and LR directions. (CT: computed tomography, CBCT: cone-beam computed tomography, sCT: synthetic computed tomography).

96.5 (2.3)% using 2%/2mm gamma-criteria and mean (SD) dose differences of −0.1 (0.2)%, 0.1 (0.3)% and −0.1 (0.3)% for the prostate base, rectum and gynecological cancer patients, the dosimetric agreement was found to meet the clinical acceptance criteria. Maspero et al. [24] used a deep learning-based sCT approach and evaluated its applicability for pelvic cancer patients. They obtained pass-rates of 95.0 (2.3)%, 91.6 (3.3)% and 92.9 (3.7)% and mean dose difference of −0.1 (0.1), −0.2 (0.2) and −0.1 (0.3) for prostate, rectum and cervix cancer patients using 2%/2mm gamma-criteria, respectively. Although reporting slightly lower agreement, their results were in line with this study.

Wang et al. [21] obtained median gamma-index pass-rate of 99.9% (99.4–100.0%) and medians of the dose difference averages were 0.21 Gy (0.2–0.3 Gy). In addition, Maspero et al. [20] evaluated the feasibility of the same method used in this study (sCTb) for rectal cancer patients obtaining the mean gamma-index pass-rate of 95.2 (4.0)% and mean dose deviation of −0.3 (0.2)% of prescription dose. Liu *et al.* [22] evaluated the sCT method for gynecological cancer patients obtaining the PTV dose deviation of 0.2 (0.4) Gy for $D_{0.5cc}$ and 0.3 (0.3) Gy for $D_{99\%}$.

Liu et al. [22] and Maspero et al. [24] results showed that the dosimetric agreement was decreased for rectum and gynecological cancer patients in comparison to prostate cancer patients. According to the body outline comparison between CT and sCT, the difference increases farther away from the imaging isocentre along CC axis. However, this was unlikely due to geometric distortion, which also increases with growing distance from the isocentre, but rather due to differences between CT and MRI modalities. Thus, higher dosimetric disagreement for patients with longer PTVs in CC direction might arise from these differences. In addition to random daily variation in body outline due to breathing and positioning, it has been suggested by Persson *et al.* that systematic differences between body outlines on CT and MRI could be attributable to longer scan time causing body relaxation [30]. Additionally, according to these results the systematic difference in the abdomen could be due to abilities of the two modalities to record the breathing motion.

Interestingly, no major difference in dosimetric performance was found between bulk HU and continuous HU sCT. This implies that already four tissue classes were adequate to capture the individual variance in body composition and to produce clinically acceptable accuracy in the dose calculation for prostate cancer patients treated with EBRT. Larger differences are typically reported between continuous HU and bulk HU sCTs. Kim et al. [18] reported no significant dosimetric difference between continuous HU or bulk-HU sCTs but obtained higher gamma-index passing-rate of 97.2% vs. 94.0% for continuous sCT evaluated with 1%/1 mm gamma-criteria. Largent et al. [17] found that the mean gamma-index pass-rate for continuous HU values (99.5%) was significantly higher than that of bulk density method (96.1%). Both Kim et al. and Largent et al. used only two bulk densities: one for bone and one for soft-tissue that could explain worse dosimetric agreement in comparison to our results. In line with our earlier study, using the sCTb [26], the patient positioning accuracy was found to be at the clinically acceptable level. However, when using continuous HU values for bone, AP positioning precision was improved as compared with the bulk assignment of HU values (sCTb). This could be due to improved visualization of pubis in sCTc, as illustrated in Fig. 1.

The mean difference between bone-based positioning between CT to CBCT and sCT to CBCT was less than 0.2 mm in all directions. The result was in agreement with earlier studies reporting sub-millimeter accuracy for the bulk HU version of the used sCT method [13,20]. Here, for the first time the soft-tissue prostate positioning of a sCT method was evaluated by comparing it to the fiducial marker-based reference. No differences in the performance between CT and sCTc were observed. However, for sCTb, the differences were slightly larger in the CC and AP directions but not in LR direction. Thus, no major difference in positioning performance was found between the methods. In addition, the use of smaller slice width for sCTc could also contribute to the observed difference.

In the DRR and soft-tissue CBCT positioning studies, there were a few outlier registrations as see in Figs. 3 and 4. For the DRR registrations, the differences were greater that is expected for either CT or MRCAT registrations alone as they were affected by the random error related to DRR-to-kV registration uncertainty both for CT and MRCAT. For soft-tissue-based registrations greater than 5 mm differences have also been reported for 28% of the registrations when comparing to seed based truth [31]. Thus, our results are in line with the reported values in the literature. The large difference may result from the poor soft-tissue visibility and artifacts in CBCT images.

Increasing the FOV in the CC direction will remain a challenging task for MRI-only planning since the geometric accuracy decreases rapidly farther away from the isocentre of MRI device. Within the study population, we found that the maximal useful FOV for one station scan was 300 mm in CC direction, while for longer FOV a two-station scan is required. For the longer FOV, the image shutter prevented analysis of geometric accuracy and body outline difference. The patient motion causes artifacts in the mDIXON image that may hamper accurate detection of body outline. Increasing the FOV in the CC direction with an acceptable scan time for preventing the organ motion and more robust motion management in the abdomen region will also remain challenges for general pelvis sCT solutions and they need to be examined further.

In this study, only a subgroup of the cohort was included in the positioning study. Consequently, the number of patients per cancer group was small. However, the positioning protocol for planar kV-image to DRR registration is similar between the groups enabling general conclusions to be drawn from these results. Furthermore, for the bone registration using CBCT images the procedure is similar between various cancer groups. On the contrary, the soft-tissue-based CBCT registration is different between the groups, and thus our conclusions apply only to prostate cancer patients. Further studies are required to assess the feasibility of other cancer types.

The implanted fiducial marker-based workflow was not included in the study although it is the clinical practice for the majority of the patients at our institution and a combination of fiducial marker alignment and soft-tissue analysis is currently the most effective and widely available approach to ensuring the accuracy in image-guided EBRT of prostate [32]. The use of fiducial markers for position verification of prostate has been evaluated for the first MRCAT algorithm (sCTb) by Tyagi et al. [13]. Thus, the re-evaluation was not considered relevant since the use of continuous HU values was not expected to impact seed-based workflow. In addition, the localization of fiducial markers from MR images has been evaluated to be sufficiently accurate and comparable to CT-based fiducial marker localization [33,34].

This study advances research and supports the future clinical implementation of sCT for general pelvic anatomy. It has been shown that continuous HU sCT was required for the accurate position verification of patients, particularly when using the soft-tissue-based registration strategies. However, the method based only on four bulk HU values was dosimetrically adequate. The use of sCT for pelvic cancer patients can be used to obtain the required dosimetric and geometric accuracy.

Acknowledgments

The authors are grateful for the efforts by an application specialist Paula Lindmark (Philips MR Therapy Oy, Vantaa, Finland) and radiographers Tarja Alamäki and Sanna Vehkomäki (Department of Oncology and Radiotherapy, Turku University Hospital, Turku, Finland) for performing the manual registrations required for the positioning study. They would also like to thank Eliisa Löyttyniemi, PhD, (Department of Biostatistics, University of Turku, Turku, Finland) for help in statistical analysis of the manuscript. In addition, we would like to show our gratitude to Lizette Warner, PhD, Head of Clinical Science, MR Oncology, Philips, for overall management of the collaboration.

Conflicts of interest

Authors Alvin Eufemio, Aleksi Halkola, Reko Kemppainen and Mark Pesola declare that they were employed by Philips MR Therapy Oy (Vantaa, Finland) by the time of conducting the research. In addition, Turku University Hospital and Philips have a contract for research collaboration.

Appendix A. Supplementary data

Supplementary data to this article can be found online at https://doi.org/10.1016/j.phro.2019.06.001.

References

[1] Dimopoulos JCA, Schard G, Berger D, Lang S, Goldner G, Helbich T, et al. Systematic evaluation of MRI findings in different stages of treatment of cervical cancer: potential of MRI on delineation of target, pathoanatomic structures, and organs at risk. Int J Radiat Oncol Biol Phys 2006;64:1380–8.

[2] Gwynne S, Mukherjee S, Webster R, Spezi E, Staffurth J, Coles B, et al. Imaging for target volume delineation in rectal cancer radiotherapy – a systematic review. Clin Oncol (R Coll Radiol) 2012;24:52–63.

[3] Hoskin P, De Bari B, Bossi A, Villeirs G, Fonteyne V, Pieters BR, et al. ESTRO ACROP consensus guideline on CT- and MRI-based target volume delineation for primary radiation therapy of localized prostate cancer. Radiother Oncol 2018;127:49–61.

[4] Schmidt MA, Payne GS. Radiotherapy planning using MRI. Phys Med Biol 2015;60:R323–61.

[5] Metcalfe P, Liney GP, Holloway L, Walker A, Barton M, Delaney GP, et al. The potential for an enhanced role for MRI in radiation-therapy treatment planning. Technol Cancer Res Treat 2013;12:429–46.

[6] Chandarana H, Wang H, Tijssen RHN, Das IJ. Emerging role of MRI in radiation therapy. J Magn Reson Imaging 2018;48:1468–78.

[7] Dirix P, Haustermans K, Vandecaveye V. The value of magnetic resonance imaging for radiotherapy planning. Semin Radiat Oncol 2014;24:151–9.

[8] Nyholm T, Nyberg M, Karlsson MG, Karlsson M. Systematisation of spatial uncertainties for comparison between a MR and a CT-based radiotherapy workflow for prostate treatments. Radiat Oncol 2009;4:54.

[9] Owrangi AM, Greer PB. Glide-Hurst CK. MRI-only treatment planning: benefits and challenges. Phys Med Biol 2018;63.

[10] Johnstone E, Wyatt JJ, Henry AM, Short SC, Sebag-Montefiore D, Murray L, et al. Systematic review of synthetic computed tomography generation methodologies for use in magnetic resonance imaging-only radiation therapy. Int J Radiat Oncol Biol Phys 2018;100:199–217.

[11] Edmund JM, Nyholm T. A review of substitute CT generation for MRI-only radiation therapy. Radiat Oncol 2017;12:28.

[12] Siversson C, Nordström F, Nilsson T, Nyholm T, Jonsson J, Gunnlaugsson A, et al. Technical Note: MRI only prostate radiotherapy planning using the statistical decomposition algorithm. Med Phys 2015;42:6090–7.

[13] Tyagi N, Fontenla S, Zhang J, Cloutier M, Kadbi M, Mechalakos J, et al. Dosimetric and workflow evaluation of first commercial synthetic CT software for clinical use in pelvis. Phys Med Biol 2017;62:2961–75.

[14] Christiansen RL, Jensen HR, Brink C. Magnetic resonance only workflow and validation of dose calculations for radiotherapy of prostate cancer. Acta Oncol 2017;56:787–91.

[15] Kemppainen R, Suilamo S, Tuokkola T, Lindholm P, Deppe MH, Keyriläinen J. Magnetic resonance-only simulation and dose calculation in external beam radiation therapy: a feasibility study for pelvic cancers. Acta Oncol 2017;56:792–8.

[16] Korhonen J, Kapanen M, Keyriläinen J, Seppälä T, Tenhunen M. A dual model HU conversion from MRI intensity values within and outside of bone segment for MRI-based radiotherapy treatment planning of prostate cancer. Med Phys 2014;41.011704.

[17] Largent A, Barateau A, Nunes JC, Lafond C, Greer PB, Dowling JA, et al. Pseudo-CT generation for MRI-only radiation therapy treatment planning: comparison among patch-based, atlas-based, and bulk density methods. Int J Radiat Oncol Biol Phys 2019;103:479–90.

[18] Kim J, Garbarino K, Schultz L, Levin K, Movsas B, Siddiqui MS, et al. Dosimetric evaluation of synthetic CT relative to bulk density assignment-based magnetic resonance-only approaches for prostate radiotherapy. Radiat Oncol 2015;10:239.

[19] Farjam R, Tyagi N, Deasy JO, Hunt MA. Dosimetric evaluation of an atlas-based synthetic CT generation approach for MR-only radiotherapy of pelvis anatomy. J Appl Clin Med Phys 2019;20:101–9.

[20] Maspero M, Tyyger MD, Tijssen RHN, Seevinck PR, Intven MPW, van den Berg CAT. Feasibility of magnetic resonance imaging-only rectum radiotherapy with a commercial synthetic computed tomography generation solution. Phys Imag Radiat Oncol 2018;7:58–64.

[21] Wang H, Du K, Qu J, Chandarana H, Das IJ. Dosimetric evaluation of magnetic resonance-generated synthetic CT for radiation treatment of rectal cancer. PLoS ONE 2018;13:1–15.

[22] Liu L, Jolly S, Cao Y, Vineberg K, Fessler JA, Balter JM. Female pelvic synthetic CT generation based on joint intensity and shape analysis. Phys Med Biol 2017;62:2935–49.

[23] Katz LM, Wang H, Duckworth T, Kim D, Das IJ, Lymberis SC. Use of synthetic CT for magnetic resonance-only based external beam pelvic radiation therapy of cervical cancer. Int J Radiat Oncol 2017;99:E676–7.

[24] Maspero M, Savenije MHF, Dinkla AM, Seevinck PR, Intven MPW, Jurgenliemk-Schulz IM, et al. Dose evaluation of fast synthetic-CT generation using a generative adversarial network for general pelvis MR-only radiotherapy. Phys Med Biol 2018;63:1–14.

[25] Köhler M, Vaara T, Van Grootel M, Hoogeveen R, Kemppainen R, Renisch S. White paper: MR-only simulation for radiotherapy planning. Philips 2015:1–16.

[26] Kemppainen R, Vaara T, Joensuu T, Kiljunen T. Accuracy and precision of patient positioning for pelvic MR-only radiation therapy using digitally reconstructed radiographs. Phys Med Biol 2018;63. aaad21.

[27] Klein S, Staring M, Murphy K, Viergever MA, Pluim JPW. Elastix: a toolbox for intensity-based medical image registration. IEEE Trans Med Imaging. 2010;29:196–205.

[28] Maspero M, Seevinck PR, Schubert G, Hoesl MAU, van Asselen B, Viergever MA, et al. Quantification of confounding factors in MRI-based dose calculations as applied to prostate IMRT. Phys Med Biol 2017;62:010.

[29] Andreasen D, Van Leemput K, Edmund JM. A patch-based pseudo-CT approach for MRI-only radiotherapy in the pelvis. Med Phys 2016;43:4742–52.

[30] Persson E, Gustafsson C, Nordström F, Sohlin M, Gunnlaugsson A, Petruson K, et al. MR-OPERA: a multicenter/multivendor validation of magnetic resonance imaging-only prostate treatment planning using synthetic computed tomography images. Int J Radiat Oncol Biol Phys 2017;99:692–700.

[31] Barney BM, Lee RJ, Handrahan D, Welsh KT, Cook JT, Sause WT. Image-guided radiotherapy (IGRT) for prostate cancer comparing kV imaging of fiducial markers with cone beam computed tomography (CBCT). Int J Radiat Oncol Biol Phys 2011;80:301–5.

[32] O'neill AGM, Jain S, Hounsell AR, O'sullivan JM. Fiducial marker guided prostate radiotherapy: a review. Br J Radiol 2016;89:1–18.

[33] Jonsson JH, Garpebring A, Karlsson MG, Nyholm T. Internal fiducial markers and susceptibility effects in MRI-simulation and measurement of spatial accuracy. Int J Radiat Oncol Biol Phys 2012;82:1612–8.

[34] Maspero M, Seevinck PR, Willems NJW, Sikkes GG, de Kogel GJ, de Boer HCJ, et al. Evaluation of gold fiducial marker manual localisation for magnetic resonance-only prostate radiotherapy. Radiat Oncol 2018;13:1–12.